Cloud feedbacks in MRI-ESM2

Hideaki Kawai (h-kawai@mri-jma.go.jp), **Tsuyoshi Koshiro, and Seiji Yukimoto**
Meteorological Research Institute, JMA

1. Introduction

The cloud feedbacks in MRI-ESM2 (Yukimoto et al. 2019), which was used for CMIP6 simulations, are briefly investigated. Changes in the vertical profiles of cloud radiative effect (CRE), cloud cover, liquid and ice water content, and number concentrations of cloud droplets and ice crystals are examined. These profile changes are examined for several areas with typical cloud regimes to understand the contributions from each cloud regime to the global cloud feedback.

2. Model and Experiments

The model resolution is TL159L80. Averages over 36 years (1979−2014) of data from amip and amip-p4K (amip with SST increased uniformly by 4 K) runs are used for the analysis. Data from amip and amip-p4K experiments with the convection scheme switched off, which were run under the second version of the project SPOOKIE (Selected Process On/Off Klima Intercomparison Experiment; Webb et al. 2015), are also examined to understand the roles of convection schemes in the cloud feedback in MRI-ESM2.

3. Results

3.1. Overview

The cloud feedback in MRI-ESM2 for shortwave (SW) radiation is +0.27 W/m^2/K, and that for longwave (LW) is −0.17, with the sum being +0.10 W/m^2/K. As is well known, the CRE changes in LW (Fig. 1a) and SW radiation (Fig. 1b) at the top of the atmosphere (TOA) tend to cancel each other out for high-level cloud areas, and the CRE changes in the sum of SW and LW radiation (Fig. 1c) reflect the changes in SW components, especially over low-level cloud areas. In addition, high-level cloud changes (Fig. 1d) correspond well to the LW changes (Fig. 1a), and low-level cloud changes (Fig. 1f) correspond well to the SW changes (Fig. 1b).

3.2. Vertical profile analysis

To understand the CRE changes, we perform a vertical profile analysis for CRE.

We focus on the SW component in this report. The approximate CRE (W/m^2) of clouds between the surface z_0 and height z for upward SW radiation, CRE_SW↑($z - z_0$), is estimated as follows:

CRE_SW↑($z - z_0$) ≈ (SW↑(all sky, z) − SW↑(clear sky, z)),

where SW↑ denotes the upward SW radiative flux (the sign is positive for net downward; Fig. 2a). In this formula, the radiative effect of clouds between TOA and z_0 to the downward SW flux is also implicitly included. To eliminate this effect, the term −(SW↑(all sky, z_0) − SW↑(clear sky, z_0)) should be added to the right-hand side (Kawai et al. 2016). By differentiating the profiles vertically, the detailed contribution of cloud at each level to the CRE can be obtained (Fig. 2b). The contribution of clouds to SW cloud feedback can be roughly estimated from the difference between the amip-p4K and amip simulations of the profiles of the contributions to CRE_SW↑($z - z_0$) (Fig. 2c).

Figure 2c shows that the vertical profile of the contribution to the CRE change for upward SW radiation is negative at levels of 100–200, 300–500, and ~800 hPa, and positive for 750–500 and ~900 hPa.

Figure 3 shows the vertical profiles of the contribution of the CRE changes for several areas with typical cloud regimes. The global positive CRE change around 900 hPa is consistent with the positive CRE change off Peru (subtropical stratocumulus area) and near Easter Island (shallow convection area). The global negative CRE change around 800 hPa is consistent with the negative CRE change near Easter Island (shallow convection area).

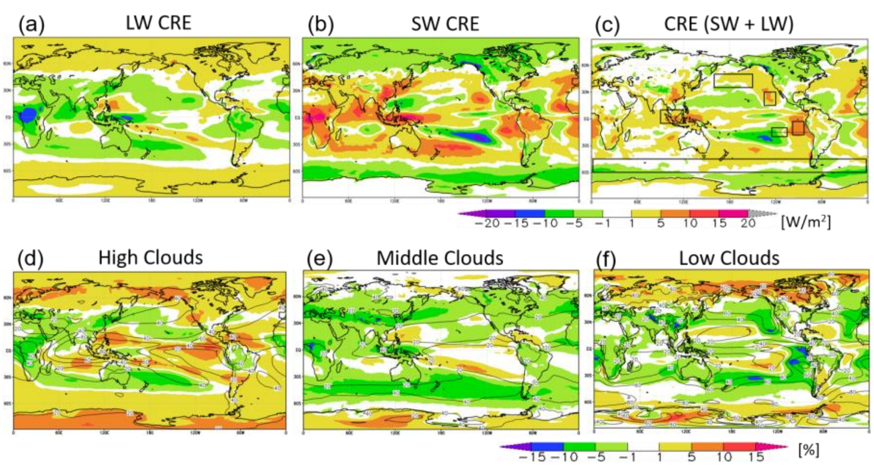

Fig. 1: Changes in CRE (amip-p4K − amip; shading) for LW (a), SW (b), and the sum of SW and LW radiation (c) at TOA, together with changes in high- (d), mid- (e), and low-level cloud cover (f). Contours are amip climatologies. MRI-ESM2 is used and the climatologies cover the period 1979–2014.

The global positive CRE change at 750–500 hPa is consistent with those near Indochina (deep convection area) and over the Southern Ocean (mid-latitude ocean). The global negative CRE change at 100–200 hPa is consistent with that near Indochina (deep convection area), and the increase in the altitude of high clouds over this region contributes to this positive CRE change. The increase in high-level clouds shown in Fig. 1d and the decrease in mid-level clouds in Fig. 1e may be partly attributed to the increase in the altitudes of high cloud layers and the cloud peak at the melting layer, and drying of the mid-level troposphere.

The noticeable reduction in the number concentration of cloud droplets and ice crystals found in MRI-CGCM3 (Kawai et al. 2015) does not occur in MRI-ESM2. The noticeable reduction in the number concentration of cloud droplets in MRI-CGCM3 was caused by a bug in the number concentration calculation.

3.3. Change in Low Clouds

Figure 1f shows that low-level clouds decrease over subtropical stratocumulus areas off the west coast of the continents. Figure 4 shows the cross-section across 15°S off Peru. Figure 4a–b clearly shows that the stratocumulus deck off Peru decreases at levels below the 850 hPa level and cumulus cloud increases above the 850 hPa level far from the coast. When the convection scheme is turned off (Fig. 4c–d), the stratocumulus deck spreads farther westward because ventilation of humidity in the boundary layer to the free atmosphere by convection does not occur. The significant reduction of the stratocumulus deck in the warmer climate is even more remarkable in the convection-off case. In MRI-ESM2, the cloud top mixing and shallow convection are suppressed when ECTEI (Estimated cloud-top entrainment index; Kawai et al. 2017) is large. Because ECTEI decreases in the future climate (Kawai et al. 2017, 2019, Koshiro et al. 2022), this parameterization may contribute to the reduction in low-level clouds in the warmer climates.

Acknowledgements

This work was partly supported by the Integrated Research Program for Advancing Climate Models (TOUGOU) Grant Number JPMXD0717935561 from the Ministry of Education, Culture, Sports, Science and Technology (MEXT), Japan. It was also supported by the Japan Society for the Promotion of Science (JSPS) KAKENHI (Grant Nos. JP18H03363, JP19K03977, and JP19H05699), and the Environmental Restoration and Conservation Agency, Japan (the Environment Research and Technology Development Fund (Grant No. 2-2003)).

References

Kawai, H., T. Koshiro, and M. J. Webb, 2017: *J. Climate*, **30**, 9119–9131.

Kawai, H., et al., 2015: *CAS/JSC WGNE Research Activities in Atmospheric and Oceanic Modelling/WMO*, **45**, 7.11-7.12.

Kawai, H., et al., 2016: *Atmos. Sci. Let.*, **17**, 548-555.

Kawai, H., et al., 2019: *Geosci. Model Dev.*, **12**, 2875–2897.

Koshiro, T., H. Kawai, and A. T. Noda, 2022: *Proc. Natl. Acad. Sci. USA*, submitted.

Webb, M. J., et al., 2015: *Phil. Trans. R. Soc. A*, **373**, 20140414.

Yukimoto, S., et al., 2019: *J. Meteor. Soc. Japan*, **97**, 931–965.

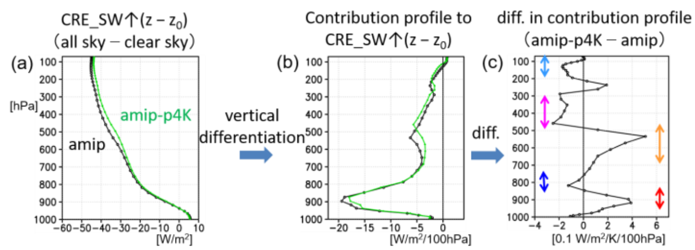

Fig. 2: (a) Cloud radiative effect (W/m^2) of clouds between the surface z_0 and height z for upward SW radiation, CRE_SW↑($z - z_0$) (black line corresponds to amip and green line amip-p4K), (b) vertical differentiation of the profiles shown in (a) that corresponds to the contribution of cloud at each level to the CRE, and (c) the difference in the contribution profiles between the amip-p4K and amip simulations shown in (b) that is normalized by 2m temperature increase. Note that $(\mathrm{CRE\_SW}\uparrow(z_{TOA})_{\text{amip-p4K}} - \mathrm{CRE\_SW}\uparrow(z_{TOA})_{\text{amip}})/\Delta T_{2m}$ corresponds to the SW cloud feedback. Model level data are used.

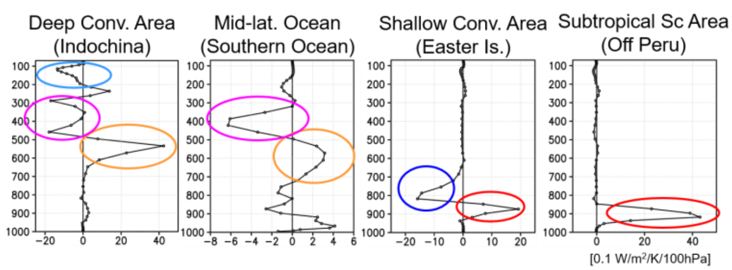

Fig. 3: Same as Fig. 2c but for the deep convection area (near Indochina), mid-latitude ocean (the Southern Ocean), shallow convection area (near Easter Island), and subtropical area (off Peru) shown in Fig.1c.

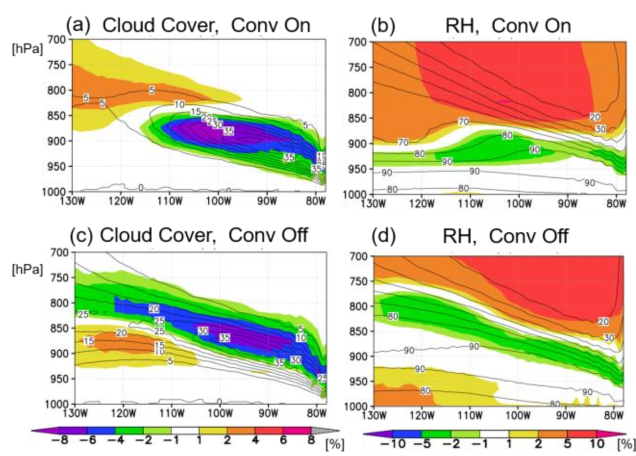

Fig. 4: Cross-sections of cloud cover (a, c) and relative humidity (b, d) along 15°S (line in Fig. 1c) (shading: difference between amip-p4K and amip; contours: amip climatology). Results of the normal model (a, b) and the convection switched off version (c, d) are shown.